Catalysis Today 150 (2010) 77–83

Contents lists available at ScienceDirect

Catalysis Today

journal homepage: www.elsevier.com/locate/cattod

Properties of CMK-8 carbon replicas obtained from KIT-6 and pyrrole at various contents of ferric catalyst

Maria Lezanska [a,*], Jerzy Wloch [a], Grzegorz Szymański [a], Ilona Szpakowska [a], Jan Kornatowski [a,b]

[a] Faculty of Chemistry, Nicolaus Copernicus University, 7 Gagarin St., 87-100 Torun, Poland
[b] Max-Planck-Institut fuer Kohlenforschung, Muelheim an der Ruhr, Germany

ARTICLE INFO

Article history:
Available online 28 July 2009

Keywords:
Carbon replicas
KIT-6
Ordered mesoporous materials
Nitrogen-containing carbons
Sorption properties
$FeCl_3$ catalyst
Liquid phase SO_2 oxidation

ABSTRACT

The CMK-8 carbons were synthesised using two KIT-6 silica matrices exhibiting well-ordered structures. With increasing synthesis temperature, the BET surface area and micropore volume diminished while the average size of mesopores increased. Among the replicas of KIT-6(1 2 0), the one synthesised using the largest amount of $FeCl_3$ (2.00 g/g silica) showed the best structure ordering. The opposite trend was observed for carbons derived from KIT-6(1 0 0): the replica prepared with use of 0.75 g $FeCl_3$/g silica exhibited the best structure ordering, reflected in the narrowest pore size distribution (centred at 4.3 nm), a_0 = 20.54 nm, and S_{BET} = 1313 m^2/g. This was due to an appropriate geometric relationship between the pore size and wall thickness of the matrix. The replicas of KIT-6(1 2 0) appeared to have a more homogenous pseudo-graphitic character. All the replicas exhibited high catalytic activity in oxidation of SO_2 in a liquid phase. The catalytic activity process does not directly correlate with the total nitrogen content; it relates to nitrogen of the quaternary type and depends on external surface areas of the samples studied.

1. Introduction

The CMK-8 carbons are replicas prepared from pyrrole similarly to the CMK-3 carbons [1]. Simultaneous presence of carbon, nitrogen, and iron in catalysts is beneficial for generating active sites appropriate for oxygen reduction [2]. For example, carbons prepared by pyrolysis of a furan resin mixed with phthalocyanine, containing nitrogen atoms in particular chemical environments, exhibit an enhanced activity in the oxygen reduction [3]. Formation of such active sites during the carbon synthesis via pyrrole polymerisation and subsequent carbonisation is possible as well.

A number of papers on preparation of carbons from polypyrrole have been published by now [4]. This precursor has also been used to synthesise replicas of micro/mesoporous matrices [5–8]. Most of these replicas were obtained from the SBA-15 matrix [5,6,8]. However, there are no reports on the synthesis of CMK-8 type carbons from polypyrrole.

The CMK-8 materials are the carbons synthesised using the KIT-6 silica matrix. KIT-6 as well as MCM-48 belong to the cubic system and to the same *Ia*3*d* space group. This three-dimensional (3D) structure facilitates the mass transfer kinetics in adsorption-based applications [9] and is beneficial for obtaining the carbon replicas. The diameter of the MCM-48 main pores is usually narrower than that of KIT-6. The other difference between these two structures is that KIT-6 exhibits an additional pore system connecting the main pores. Due to that, formation of a stable faithful replica of KIT-6 should be possible, as it is in the case of the materials pair SBA-15/CMK-3. Lack of such a porous system in MCM-48 results in a less-ordered replica structure ($I4_132$) obtained after removal of silica [10]. The 3D ordered mesoporous silica applied as a matrix in the synthesis of the carbon replicas seems to provide sufficient accessibility to $FeCl_3$ used as a catalyst for the pyrrole polymerisation.

In the presented method for the replica synthesis with use of controlled amounts of $FeCl_3$, carbon materials of various pore sizes, pore volumes, and surface areas were obtained. After carbonisation of the carbon–silica composites, the samples were washed with the HF and HCl solutions and with water to remove silica and residual Fe.

The aim of this study was to estimate the influence of (i) the amount of introduced $FeCl_3$ as the catalyst for pyrrole polymerisation and (ii) use of two matrices of different pore diameters (7.4 and 8.4 nm, BJH_{des}) on sorption properties of the CMK-8 replicas. It is known from the literature, that nitrogen-containing carbons are active in the SO_2 oxidation [11–14]. However, the results about the effect of the total nitrogen content and of the contents of particular nitrogen forms on the catalytic activity of the carbon materials are

* Corresponding author. Tel.: +48 56 611 47 52; fax: +48 56 654 24 77.
E-mail address: miriam@chem.uni.torun.pl (M. Lezanska).

0920-5861/$ – see front matter © 2009 Elsevier B.V. All rights reserved.
doi:10.1016/j.cattod.2009.06.020

inconsistent. Thus, catalytic properties of the obtained carbons were tested in the reaction of the SO_2 oxidation performed in an aqueous solution. The influences of the ordering of the carbon pore structure and of the nitrogen content on the rate of the SO_2 oxidation process were also studied.

2. Experimental

The KIT-6 parent materials were obtained after a slightly modified procedure reported by Kim et al. [15]. According to this, the gel of the following molar composition: 0.017 P123:1.2 TEOS:1.31 BuOH:1.83 HCl:195 H_2O was applied. Two matrices, KIT-6(1 0 0) and KIT-6(1 2 0), were synthesised at 373 and 393 K, respectively. The CMK-8 replicas were prepared similarly as CMK-3 [8], using pyrrole and $FeCl_3$ as the polymerisation catalyst. They were also similarly washed with solutions of HF and HCl and with deionised water. The carbons are denoted as C*x*NKIT-6(1 0 0) and C*x*NKIT-6(1 2 0), where *x* is the number of g $FeCl_3$ (0.75, 1.25, and 2.00) per 1 g of KIT-6. The matrices and replicas were characterised by XRD, nitrogen adsorption, thermal analysis, and TEM with EDX. Sorption isotherms were determined with a Micromeritcs ASAP 2010 volumetric analyser. Structure properties were examined using a Philips X'Pert PRO System. TGA and DTA profiles were recorded with a TA Instruments SDT 2960 apparatus. The catalytic activity was measured at 294 K using a batch reactor in an aqueous phase with a SO_2 solution of 1.65×10^{-3} M SO_2 and O_2 concentration kept constant by continuous air bubbling inside the reactor (3 dm^3/h, $[O_2] > 10^{-3}$ M). The SO_2 conversion was monitored by conductometry [12,13]. Catalytic activities of CMK-3 free of nitrogen and of CMK-3N1.25 discussed elsewhere [1] are taken into account for comparison.

3. Results and discussion

The XRD powder patterns of KIT-6(1 0 0) and KIT-6(1 2 0), being the materials with a cubic symmetry, exhibit features characteristic of the *Ia*3*d* structure (Fig. 1). The most intense peak (at $2\theta = 0.94^\circ$) of the KIT-6(1 0 0) pattern corresponds to the interplanar distance of $d_{2\,1\,1} = 9.45$ nm. The interplanar distance of KIT-6(1 2 0) is somewhat larger: $d_{2\,1\,1} = 10.08$ nm, as derived from the peak located at $2\theta = 0.88^\circ$. This indicates that the unit cell constant, a_0, of KIT-6 increases as the synthesis temperature rises.

The nitrogen sorption isotherms for the KIT-6 materials (Fig. 2) are of type IV, each with a hysteresis loop of type H_1 occurring at $p/p_s = 0.65$–0.80. Filling the pores of KIT-6(1 2 0) begins at $p/p_s = 0.75$, compared to $p/p_s = 0.70$ for KIT-6(1 0 0). The hysteresis loop for KIT-6(1 2 0) appears at higher values of p/p_s (0.75–0.80) in relation to that for KIT-6(1 0 0), which suggests that pore diameters of the former material are larger. Structural parameters derived from the α_s plots (Table 1) indicate that the micropore volume of KIT-6(1 0 0) is larger (0.06 cm^3/g) and the mesopore volume is smaller (0.98 cm^3/g) as compared to KIT-6(1 2 0) (0.01 and 1.08 cm^3/g, respectively). The BET surface areas are 781 and 698 m^2/g for KIT-6(1 0 0) and KIT-6(1 2 0), correspondingly. The pore diameters, calculated by the BJH method from the adsorption branches of the isotherms, are 8.91 and 9.77 nm (Fig. 3) while those derived from the desorption branches, 7.35 and 8.39 nm for KIT-6(1 0 0) and KIT-6(1 2 0), respectively. One can conclude that the volume and average diameter of mesopores increase while the volume of micropores slightly decreases as the synthesis temperature rises.

After impregnation with $FeCl_3$, sorption capacity of KIT-6 decreases, although the isotherm shape (type IV) and position of the hysteresis loop are preserved (Fig. 2b). This indicates that a fraction of pores is blocked, some pores remaining unfilled.

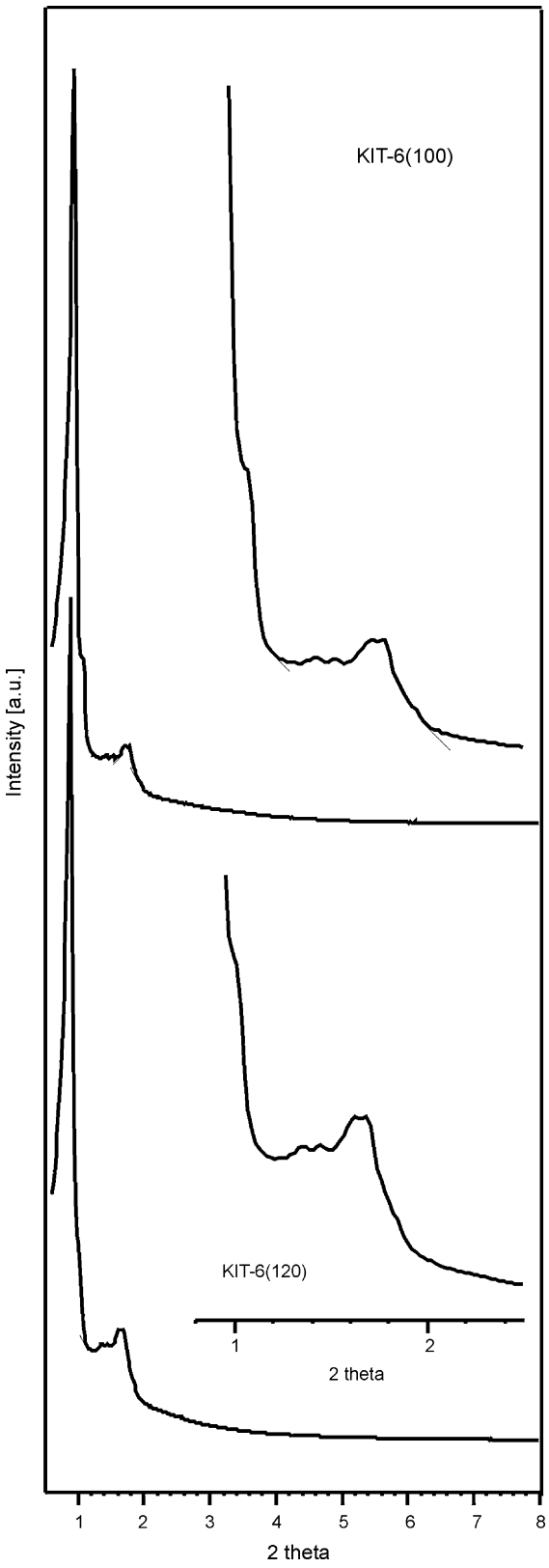

Fig. 1. XRD powder patterns of KIT-6(1 0 0) and KIT-6(1 2 0) matrices.

The prepared mesoporous carbons exhibit different structure ordering. Lack of peaks within the 2θ range of 0.6–7.5° in the XRD patterns of C0.75NKIT-6(1 2 0) and C1.25NKIT-6(1 2 0) does not unequivocally prove that an ordered mesoporous phase is absent in these materials (Fig. 4a). It is possible that a broad peak

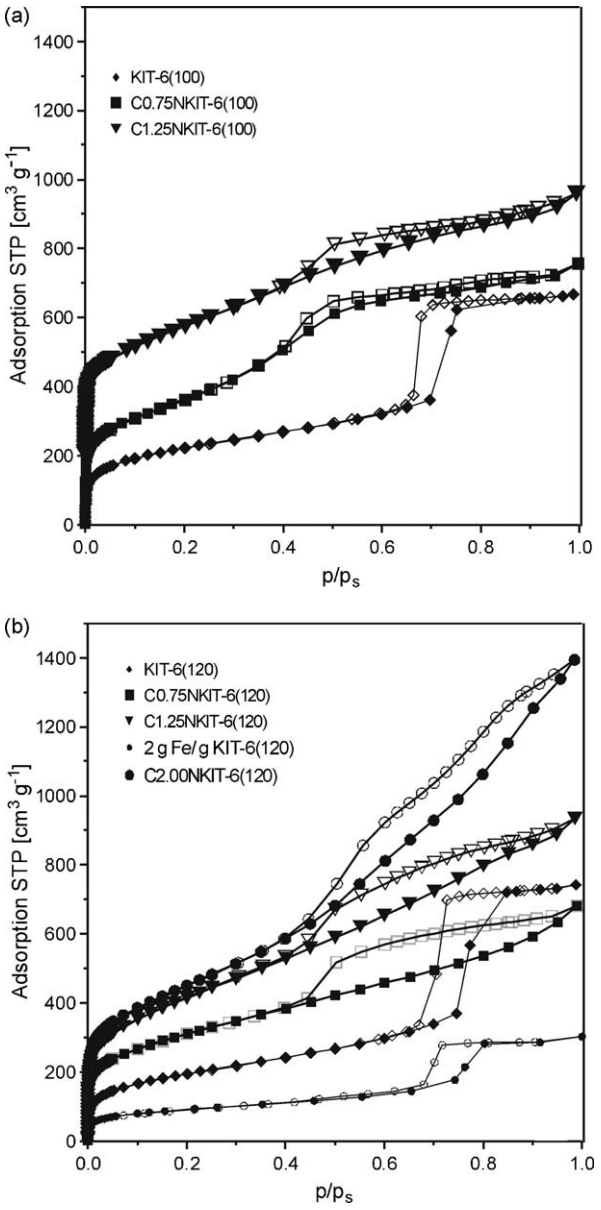

Fig. 2. Nitrogen sorption isotherms for (a) KIT-6(1 0 0) and its carbon replicas and (b) KIT-6(1 2 0) and its replicas. Adsorption and desorption branches are marked with filled and open symbols, respectively. 2 g Fe/g KIT-6(1 2 0) denotes impregnation with 2 g of $FeCl_3$ per g of the matrix.

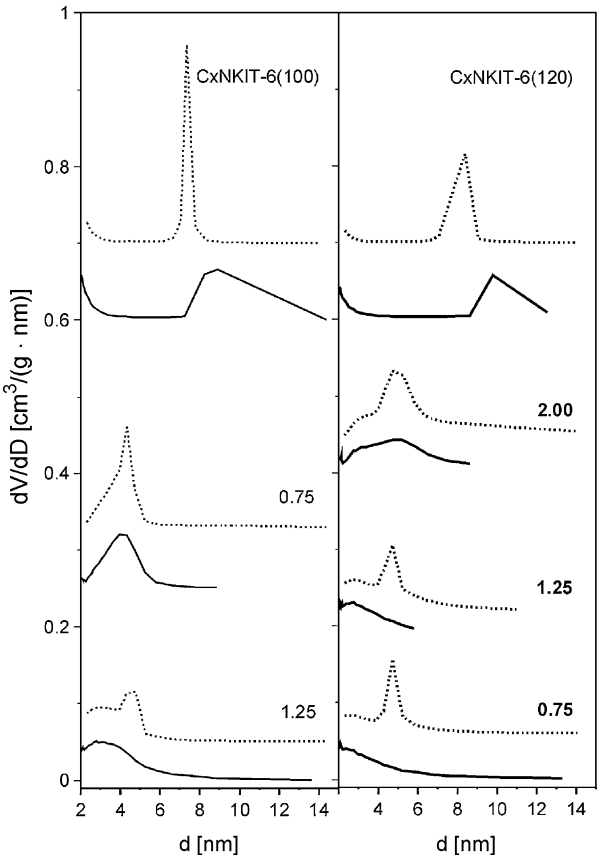

Fig. 3. Pore size distributions calculated by a modified BJH-KJS method from adsorption (solid) and desorption (dashed lines) branches of relevant isotherms. Left: KIT-6(1 0 0) and its carbon replicas; right: KIT-6(1 2 0) and its replicas. Upper curves correspond to matrices, lower ones, to replicas (numbers denote the amounts of catalyst in g $FeCl_3$ per g KIT-6). For clarity, the PSD curves, except those for C1.25NKIT-6(1 0 0) and C0.75NKIT-6(1 2 0), are shifted up along the *y* axis.

attributed to a mesoporous phase exhibiting a heterogeneous structure ordering may occur below $2\theta = 0.6^\circ$. In the XRD pattern of C2.00NKIT-6(1 2 0), a small peak appears at $2\theta = 0.70^\circ$ in addition to the main peak located at $2\theta = 1.03^\circ$. This might suggest that a less-ordered ($I4_132$) or separate ($Ia3d$) phase is present in this material. The pore size distribution of this sample (Fig. 3) reveals two peaks, which seems to prove the latter possibility. The replicas of KIT-6(1 0 0) (Fig. 4a) are characterised by a good structure ordering, indicated by the peak at $2\theta = 1.05^\circ$ occurring in the patterns of both C0.75NKIT-6(1 0 0) and C1.25NKIT-6(1 0 0). Exception is the C2.00NKIT-6(1 0 0) sample that shows no reflections in the small-angle range of the XRD pattern (Fig. 4a).

Table 1
Nitrogen contents and structural parameters of KIT-6 matrices and their carbon replicas.

Sample	N content[a] (wt.%)	N–Q[a] (at.%)	V_{mi} (cm^3/g)	V_p (cm^3/g)	S_t (m^2/g)	S_{ext} (m^2/g)	S_{mez} (m^2/g)	S_{BET} (m^2/g)	$d_{BJH-KJS\ ads/des}$ (nm)
KIT-6(1 0 0)	n.d.	n.a.	0.06	0.98	657	34	623	781	8.91/7.35
KIT-6(1 2 0)	n.d.	n.a.	0.01	1.08	672	38	634	698	9.77/8.39
C0.75NKIT-6(1 0 0)	5.88	1.75	0.10	1.07	896	25	871	1313	3.94/n.a.
C1.25NKIT-6(1 0 0)	7.33	1.69	0.09	0.98	911	74	837	1355	~3.0/n.a.
C2.00NKIT-6(1 0 0)	5.98	1.88	n.d.	n.d.	n.d.	n.d.	n.d.	1	n.d.
C0.75NKIT-6(1 2 0)	7.26	2.34	0.08	0.75	781	131	651	1098	n.d./n.a.
C1.25NKIT-6(1 2 0)	4.31	1.58	0.08	1.20	1097	101	996	1491	~2.8/n.a.
C2.00NKIT-6(1 2 0)	6.65	2.62	0.08	1.65	1243	229	1014	1616	~3.0; ~5.0/n.a.

The parameters were calculated from the α_s plots (V_{mi}, micropore volumes; V_p, primary mesopore volumes; S_t, total surface areas; S_{ext}, external surface areas; S_{mes}, mesopore surface areas; S_{BET}, BET surface areas; and $d_{BJH-KJS\ ads/des}$, pore diameters derived from the adsorption/desorption branch by the BJH–KJS method); n.d., not determined; n.a., not applicable.

[a] From XPS.

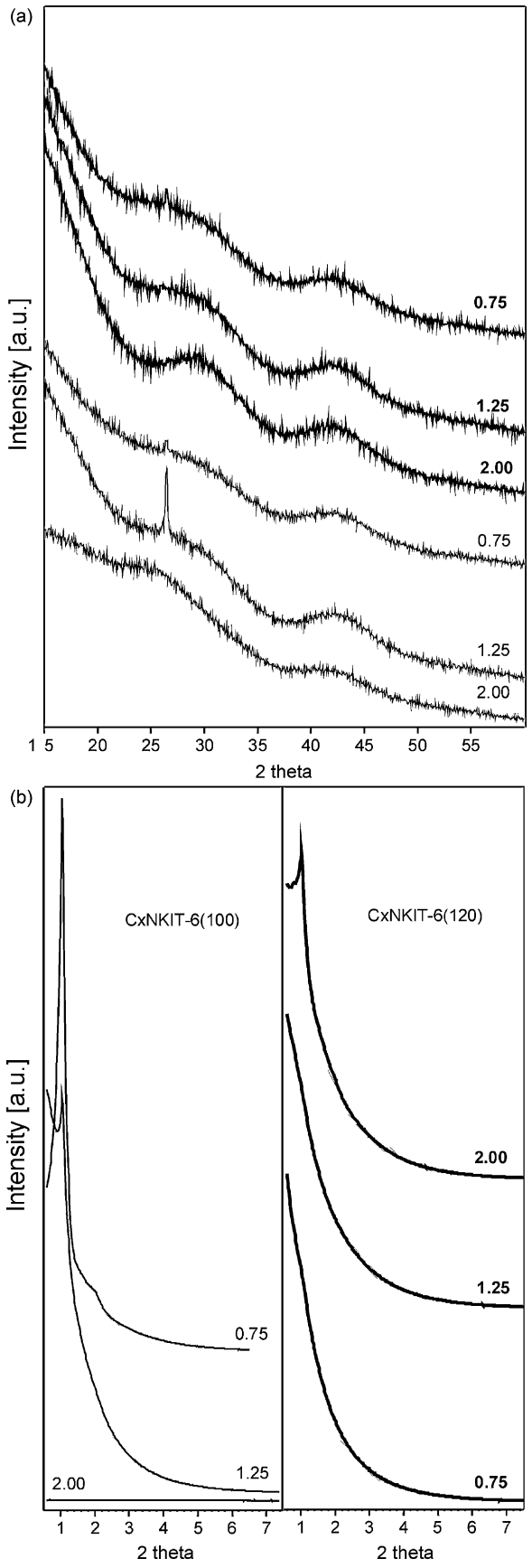

Fig. 4. XRD powder patterns of carbon replicas of KIT-6(1 0 0) and KIT-6(1 2 0) in the low (a) and high (b) angle ranges, respectively. The curves in (b) for C*x*NKIT-6(1 2 0) are distinguished with thick lines while numbers denote the amounts of catalyst in g $FeCl_3$ per g of the matrix.

In the case of C0.75NKIT-6(1 0 0), an additional peak appears at $2\theta = 2.00^\circ$. This material may be considered as the one exhibiting the best structure ordering. The $d_{2\,1\,1}$ peak (at $2\theta = 1.05^\circ$) for this sample is very intense and it corresponds to $a_0 = 20.54$ nm, the value being slightly smaller than that for the matrix (23.14 nm). The patterns in the high-angle range (Fig. 4b) show two broad peaks at $2\theta = 25–35^\circ$ and $2\theta = 37–47^\circ$, consistent with the pattern of a graphitic carbon with the peaks at $2\theta = 26.30^\circ$ ($d_{0\,0\,2}$) and $2\theta = 43.50^\circ$ ($d_{1\,0\,1}$) reported in the literature [16]. Moreover, a sharp intense peak at $2\theta = 26.48^\circ$, that is likely due to traces of $Fe_2O_3{\cdot}H_2O$ [17], appears only in the XRD pattern of C1.25NKIT-6(1 0 0). Probably, the traces of the Fe species are blocked in the bulk of this sample and cannot be removed by washing. However, the presence of Fe atoms in any sample has not been proved by XPS.

Fig. 4a indicates that each replica contains a fraction of graphitic domains. Nevertheless, the shape of the peaks does not allow one to assess this fraction quantitatively; the structure homogeneity as detected by XRD is too low. On the other hand, the TGA results (Fig. 5) show that the replicas of KIT-6(1 2 0) are structurally more homogeneous than those of KIT-6(1 0 0) because the former materials exhibit significantly narrower peaks in the range of 680–780 K on both DTG and DTA curves.

As found with XPS, the contents of C, N, and O of all the studied samples except C1.25NKIT-6(1 2 0) are similar. The nitrogen and oxygen contents are within the range of 4.31–7.33 (Table 1) and 2.72–3.54 wt.%, respectively. Interestingly, all the XPS spectra of the studied replicas prove the presence of nitrogen and oxygen, in addition to carbon that constitutes ca. 90%. No other elements have been detected in these samples, except C1.25NKIT-6(1 2 0), in which traces of Al and F were found. The fluorine atoms were possibly incorporated into the carbon structure during the matrix dissolution in HF. The reason for the presence of the Al traces in these XPS spectra is unknown. This sample contains the smallest amount of nitrogen (4.31 wt.%) and the largest one of oxygen (8.39 wt.%). In spite of similar structures of matrices, the matrix with wider pores, i.e., KIT-6(1 2 0) as compared to KIT-6(1 0 0), enables to introduce slightly higher amounts of nitrogen, into the carbon replicas in the case of 0.75 and 2.00 g of $FeCl_3$ (Table 1).

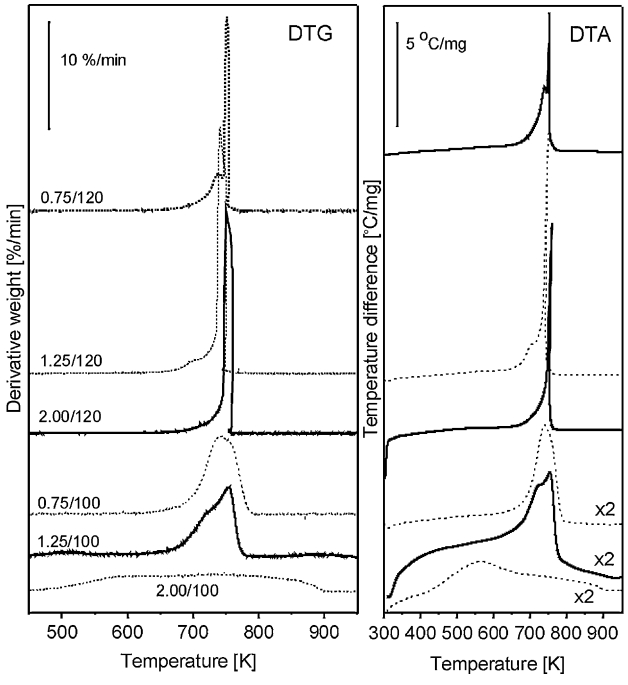

Fig. 5. Thermal analysis of the studied carbon replicas under air.

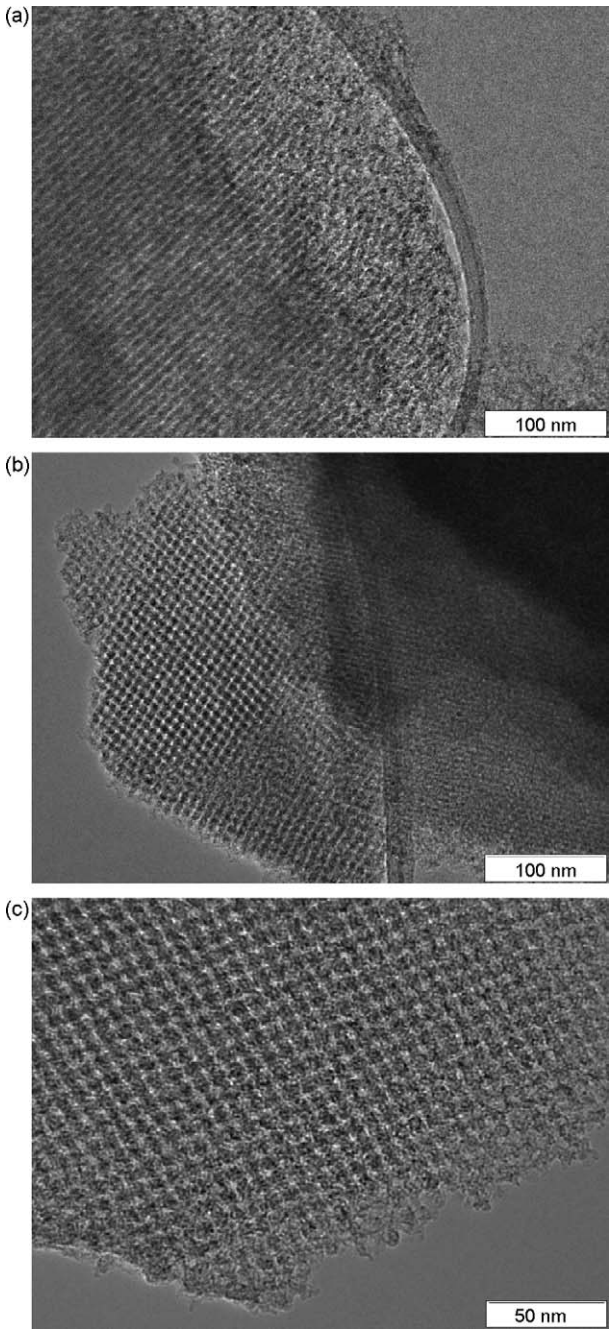

Fig. 6. TEM images of C2.00-KIT-6(1 2 0) (a) and C0.75-KIT-6(1 0 0) at various magnifications (b), (c).

The TEM images of the studied materials only show honeycomb structures and no the $I4_132$ phase (Fig. 6).

Similarly as for the matrices, the nitrogen sorption isotherms for the CMK-8 carbon replicas (Fig. 2) are of type IV, although the hysteresis loops are of mixed types. The shapes of the sorption isotherms for the nitrogen-containing replicas of KIT-6(1 2 0) depend on the amount of the introduced $FeCl_3$. The C2.00NKIT-6(1 2 0) sample exhibits the highest sorption capacity and the best structure ordering among the carbon replicas prepared from KIT-6(1 2 0) (see Fig. 6a shown as an example of good ordering). The BJH pore size distribution curve for this sample, based on the adsorption branch, includes two broad peaks situated at ca. 3 and 5 nm (Fig. 3). The BET surface area (1616 m^2/g) and mesopore volume (1.65 cm^3/g) of that material are also the highest as compared to the parameters of other replicas (Table 1). For carbons with diminishing amounts of $FeCl_3$ used to impregnate the matrix, these quantities decrease down to, respectively, 1098 m^2/g and 0.75 cm^3/g for C0.75NKIT-6(1 2 0). The latter material exhibits the largest micropore volume (0.08 cm^3/g). The average micropore diameters of all the replicas prepared using KIT-6(1 2 0) are similar to one another (1.06–1.07 nm). The BET surface areas and mesopore volumes for the carbonaceous replicas are notably larger than those for the respective siliceous matrices (Table 1). For example, the BET surface area for C2.00NKIT-6(1 2 0) (1616 m^2/g) is more than twice as much as that for KIT-6(1 2 0) (698 m^2/g). The pore size distributions for C0.75NKIT-6(1 2 0) and C1.25NKIT-6(1 2 0) are less uniform. The respective BJH curves, derived from the adsorption branches, include no peaks except a broad one situated at ca. 2.8 nm for the C1.25NKIT-6(1 2 0) sample. The hysteresis loops for these materials are of mixed types. However, most carbons exhibit clear maxima in the desorption-related pore size distributions. These maxima, located around 4 nm, could improperly be assigned to the presence of actual pores. In the cases of a broad pore size distribution, pore network effects, and cage-like structures, the desorption branch is particularly sensitive to the so-called tensile strength effect (TSE) of the adsorbed phase, leading to a forced closure of the hysteresis loop around $p/p_0 = 0.42$ for N_2 at 77 K [18]. The forced closure of the hysteresis in the critical pressure range seems to be a result of instability of the hemispherical meniscus during desorption from the pores of a critical diameter (approximately 4 nm) [19]. Thus, for hysteresis loops ending at the limiting pressure of the hysteresis closure ($p/p_0 = 0.42$ for nitrogen), the pore size distribution (PSD) cannot be determined from the desorption branch of the isotherm. However, the PSDs derived from both the adsorption and desorption branches, presented for comparison in Fig. 3, can be used as a criterion to evaluate the non-physical nature of the pores the sizes of which have been obtained from the desorption curve. The pore sizes derived from both the adsorption and desorption branches are presented for silica matrices only (Table 1). It appears that desorption from the KIT-6 matrices is not affected by the TSE phenomenon (Figs. 2 and 3).

Relatively broad distributions of pore sizes (mostly mesopore ones) of the carbon replicas result probably from the fact that $FeCl_3$ precipitates unevenly on the silica walls, which changes pore geometry of the matrices. These changes influence pore sizes and, presumably, wall thicknesses of forming carbons. In practice, when large amounts of ferric chloride are used, one can expect significant irregularities of the carbon structure. However, as shown by the nitrogen sorption investigations, sufficiently large pore diameters of matrices enable formation of stable carbonaceous replicas, in spite of large quantities of the catalyst applied. Selection of matrices with an appropriate pore diameter/wall thickness ratio, which would provide continuity of walls and uniformity of pores of replicas to be prepared, seems to be the most important factor relevant to the carbon synthesis.

In the case of the replicas of KIT-6(1 0 0), the tendency of variation in the carbon structure ordering upon the catalyst amount used to impregnate the matrix appears to be opposite to that for the replicas of KIT-6(1 2 0). When the largest amount of $FeCl_3$, i.e., 2.00 g per 1 g of KIT-6(1 0 0), was applied, then a practically non-porous carbon was obtained ($S_{BET} \leq 30$ m^2/g). Thus, the nitrogen sorption data for that sample are not shown here. Two replicas prepared with use of smaller amounts (0.75 and 1.25 g/g) of the catalyst exhibit ordered structures with pore volumes and specific surface areas similar to each other (Table 1). However, the structure ordering of C0.75NKIT-6(1 0 0) seems to be slightly better than that of C1.25NKIT-6(1 0 0).

The shape of the hysteresis loop occurring on the nitrogen sorption isotherm of C1.25NKIT-6(1 0 0) indicates the presence of

mesopores in this material (Fig. 2). The mesopore size distribution curve derived from adsorption reveals a broad peak in the range of 2.5–4.0 nm (Fig. 3). The mesopore diameters of this sample appear to be more uniform in relation to those of the replicas of KIT-6(1 2 0). The micropore size distribution is also rather broad, with an average pore diameter being 1.05 nm.

The C0.75NKIT-6(1 0 0) sample exhibits the best structure ordering among all the studied carbon replicas. In addition, the shape of its nitrogen sorption isotherm is the most similar to the shape of the type IV isotherm. The relatively high increase in adsorption at the relative pressure corresponding to the onset of the mesopore filling (Fig. 2) results in quite uniform mesopore size distributions (Fig. 3) derived from the adsorption branch (maximum at 3.94 nm). The micropore size distribution is relatively broad, with the maximum at 1.1 nm. The XRD and TEM data confirm a superior structure ordering of this sample (Fig. 6b and c).

Carbons prepared using the same relative amounts of ferric chloride, e.g., C1.25NKIT-6(1 0 0) and C1.25NKIT-6(1 2 0), are characterised by the parameter values (derived from the α_s plots) close to each other. For example, the BET surface areas are 1355 and 1491 cm^2/g for C1.25NKIT-6(1 0 0) and C1.25NKIT-6(1 2 0), respectively (Table 1). One can conclude that, although the amount of the introduced iron determines the carbon structure ordering, diameters and volume of matrix pores affect quality of the replicas as well. It turned out that the carbon materials of the best structure ordering were prepared using different amounts of $FeCl_3$ and matrices of different structure, namely C0.75NKIT-6(1 0 0) and C2.00NKIT-6(1 2 0). When a matrix with an average pore diameter of 7.35 nm was impregnated with 2.00 g/g of $FeCl_3$, the catalyst quantity appeared to be too large: the pores were filled with ferric chloride to such an extent that the amount of introduced pyrrole was insufficient to provide continuous carbonaceous walls. On the other hand, the replica prepared from a matrix of the 8.39-nm average pore diameter was of sufficient quality. The structure ordering of C0.75NKIT-6(1 2 0) is poorer than that of C0.75NKIT-6(1 0 0) because, probably, the catalyst quantity was too low in relation to the amount of pyrrole introduced into the matrix.

The prepared nitrogen-containing carbons exhibit larger pore volumes and BET surface areas as compared to the CMK-8 replicas free of nitrogen and prepared from acenaphthene or pitch. The surface areas of the latter carbons were 290–960 m^2/g while the volumes of adsorbed nitrogen did not exceed 350 cm^3 STP/g. The sample prepared from petroleum tar, with the surface area of 1250 m^2/g, was an exception. The pore size distributions for the CMK-8 samples prepared from pyrrole are mostly broader than those for the carbons containing no nitrogen [20]. This may be due to imperfections of the replication process.

Introduction of ferric chloride as a polymerisation catalyst after filling the pores of the mesoporous SBA-15 matrix with pyrrole led to obtaining a mesoporous carbon containing magnetic nanoparticles. It exhibited a uniform pore size distribution centred at 2.9 nm, but the BET surface area and the single-point total pore volume reached only 643 m^2/g and 0.6 cm^3/g, respectively [21]. The same result could be expected if such a synthesis method would be applied to KIT-6 when used as a matrix.

As expected, all the N-doped carbon samples demonstrate high catalytic activity. However, there is no explicit relation between the catalytic activity and total surface concentration of nitrogen, as observed earlier by Timpe and Schlögl for nitrogenated carbon blacks [12]. According to the XPS results [13], the incorporated nitrogen forms the following species: pyridinic (398.5 ± 0.2 eV), pyrrole/pyridine (400.5 ± 0.2 eV), quaternary (401.2 ± 0.2 eV), and oxidised nitrogen (402.9 ± 0.2 eV). As found in the present work, a correlation exists between the catalytic activity and the amount of quaternary nitrogen species (N–Q) (Fig. 7a). This is in contrast to the data by Raymundo-Piñero and

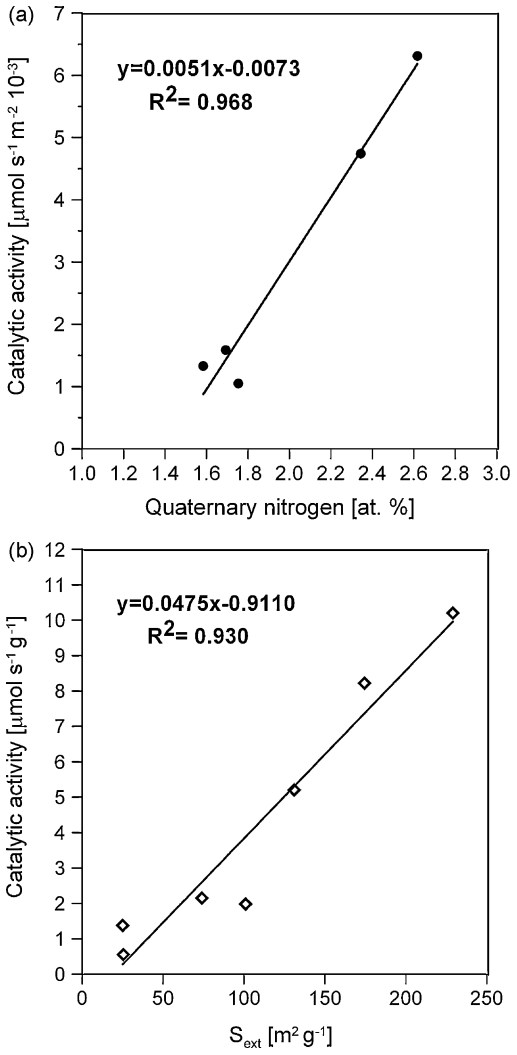

Fig. 7. Catalytic activity for SO_2 oxidation versus (a) quaternary nitrogen (N–Q) percentage and (b) external surface area of nitrogen-containing carbons studied (Table 1) and CMK-3 samples (see text). The data for the collapsed sample C2.00NKIT-6(1 0 0) are not included in (a).

Cazarola-Amorós [22] who reported a relationship between the activity and both the nitrogen content and the concentration of pyridine-like species for some carbon materials.

The term quaternary-N (N–Q) covers a number of different structures. Thus, N–Q may represent various functionalities in different materials [23]. Generally, it is assumed that quaternary nitrogen species are nitrogen atoms at different positions (top, centre, or valley) in a graphene layer as well as protonated pyridinic-like structures [11,23]. According to quantum chemical calculations, combinations of some of them, especially with oxygen structures incorporated into the graphene layer (pyrone, chromene), reveal the highest charge mobility in a carbon matrix and the best donor–acceptor properties [24,25]. The carbons with such species are more efficient in formation of the O_2^- iono-radical structures that likely control the catalytic activity of carbons in the oxidation reactions [23].

The observed (Fig. 7b) increase in the catalytic activity with increasing carbon external surface area (S_{ext}) indicates that the oxidation of SO_2 predominantly occurs on the outer surface of the carbons. Catalytic activities of two mesoporous CMK-3 carbons for this reaction are shown for comparison (Fig. 7b). One of these materials, nitrogen-free CMK-3, exhibited a relatively low external surface area (25.5 m^2/g). The other one, CMK-3N1.25 containing

5.0 wt.% of nitrogen, exhibited the external surface area of 174.4 m^2/g.

4. Conclusions

The structure ordering of the CMK-8 carbon replicas is strongly associated with the amount of a polymerisation catalyst, $FeCl_3$, and, to a lesser extent, with the pore diameter of a matrix. The synthesis of well-ordered CMK-8 replicas from pyrrole is possible if mutually appropriate type of matrix and amount of catalyst are used. The prepared carbons contain relatively high amount of nitrogen (up to 7.3%) incorporated predominantly in pyridinic and quaternary forms. The latter species are probably active sites for the SO_2 oxidation in aqueous solutions. All the materials effectively promote this process, occurring mainly on the outer surface of the carbons. The presented results suggest that the correlation between catalytic activity and external surface area may also apply to other mesoporous carbonaceous replicas containing or free of nitrogen.

References

[1] M. Lezanska, J. Wloch, J. Kornatowski, Stud. Surf. Sci. Catal. 174B (2008) 945.
[2] F. Jaouen, S. Marcotte, J.-P. Dodelet, G. Lindbergh, J. Phys. Chem. B 107 (2003) 1376.
[3] J. Ozaki, S. Tanifuji, N. Kimura, A. Furuichi, A. Oya, Carbon 44 (2006) 1324.
[4] H. Yoon, S. Ko, J. Jang, Chem. Commun. (2007) 1468;
C.-C. Han, J.-T. Lee, R.-W. Yang, C.-H. Han, Chem. Mater. 13 (2001) 2656;
C.-C. Han, J.-T. Lee, H. Chang, Chem. Mater. 13 (2001) 4180;
J. Jang, B. Lim, J. Lee, T. Hyeon, Chem. Commun. (2001) 83;
C.-C. Han, J.-T. Lee, R.-W. Yang, H. Chang, C.-H. Han, Chem. Mater. 11 (1999) 1806;
Y. Wang, F. Su, C.D. Wood, J.Y. Lee, X.S. Zhao, Ind. Eng. Chem. Res. 47 (2008) 2294;
C. Wang, D. Ma, X. Bao, J. Phys. Chem. C 112 (2008) 17596;
H. Dong, W.E. Jones Jr., Langmuir 22 (2006) 11384;
J. Jang, J.H. Oh, G.D. Stucky, Angew. Chem. Int. Ed. 41 (2002) 4016.
[5] P.F. Fulvio, M. Jaroniec, C. Liang, S. Dai, J. Phys. Chem. C 112 (2008) 13126.
[6] A.B. Fuertes, T.A. Centeno, J. Mater. Chem. 15 (2005) 1079.
[7] A. Garsuch, R.R. Sattler, S. Witt, O. Klepel, Micropor. Mesopor. Mater. 89 (2006) 164.
[8] C.-M. Yang, C. Weidenthaler, B. Spliethoff, M. Mayanna, F. Schueth, Chem. Mater. 17 (2005) 355.
[9] K. Schumacher, M. Grun, K.K. Unger, Micropor. Mesopor. Mater. 27 (1999) 201.
[10] R. Ryoo, S.H. Joo, S. Jun, J. Phys. Chem. B 103 (1999) 7743.
[11] J. Lahaye, G. Nanse, A. Bargeev, V. Strelko, Carbon 37 (1999) 585.
[12] O. Timpe, R. Schlögl, Ber. Bunsenges. Phys. Chem. 97 (1993) 1076.
[13] E. Raymundo-Piñero, D. Cazarola-Amorós, A. Linares Solano, Carbon 41 (2003) 1925.
[14] K. Li, L. Ling, C. Lu, W. Qiao, Z. Liu, L. Liu, I. Mochida, Carbon 39 (2001) 1803.
[15] T.-W. Kim, F. Kleitz, B. Paul, R. Ryoo, J. Am. Chem. Soc. 127 (2005) 7601.
[16] Y. Xia, R. Mokaya, Adv. Mater. 16 (2004) 886.
[17] Philips Database X'Pert High Score, reference code: 00-003-0430.
[18] J.C. Groen, J. Perez-Ramirez, Appl. Catal. A: Gen. 268 (2004) 121.
[19] J.C. Groen, L.A.A. Peffer, J. Perez-Ramirez, Micropor. Mesopor. Mater. 60 (2003) 1.
[20] K.P. Gierszal, T.-W. Kim, R. Ryoo, M. Jaroniec, J. Phys. Chem. 109 (2005) 23263.
[21] J. Lee, S. Jin, Y. Hwang, J.-G. Park, H.M. Park, T. Hyeon, Carbon 43 (2005) 2536.
[22] E. Raymundo-Piñero, D. Cazarola-Amorós, J. Chem. Educ. 76 (7) (1999) 958.
[23] J.R. Pels, F. Kapteijn, J.A. Moulijn, Q. Zhu, K.M. Thomas, Carbon 33 (11) (1995) 1641.
[24] V.V. Strelko, N.T. Kartel, I.N. Dukhno, V.S. Kuts, R.B. Clarkson, B.M. Odintsov, Surface Sci. 548 (2004) 281.
[25] V.V. Strelko, V.S. Kuts, P.A. Thrower, Carbon 38 (2000) 1499.